

Article

Experimental Validation of Finite Element Models for Open-to-CHS Column Connections

Rajarshi Das ^{1,*}, Alper Kanyilmaz ² and Herve Degee ¹ 

¹ Construction Engineering Research Group, Hasselt University, 3590 Diepenbeek, Belgium; herve.degee@uhasselt.be

² Department of Architecture, Built Environment and Construction Engineering, Politecnico di Milano, 20133 Milan, Italy; alper.kanyilmaz@polimi.it

* Correspondence: rajarshi.das@uhasselt.be

Abstract: The conventional ways to construct an open-to-circular hollow section (CHS) connection are either to directly weld the open section to the CHS column wall or to use local stiffeners (e.g., diaphragms) and gusset plates to connect the two structural components. These construction methods often subject the CHS to severe local distortions and/or require high welding quantities, hindering the real-life application of hollow sections. To overcome such difficulties, this study proposes two types of moment-resisting “passing-through” connection configurations, developed within the European research project “LASTEICON”. These configurations consist of main beams connected to the CHS column via either an I-section or individual steel plates passing through the CHS column. The passing-through system is implemented using laser cut and weld technology and efficiently avoids excessive use of stiffening plates, local damages on the CHS wall and premature flange failures. The proposed configurations are investigated experimentally and numerically under two different load cases in order to characterize their structural behaviour. Finite element models have been developed and calibrated with respect to the experimental force–displacement behaviour of the connections as well as their observed failure modes. The efficiency, benefits, and limitations of the modelling approach were discussed through a detailed comparison study between the experimental and numerical results.



Citation: Das, R.; Kanyilmaz, A.; Degee, H. Experimental Validation of Finite Element Models for Open-to-CHS Column Connections. *Modelling* **2023**, *4*, 454–469. <https://doi.org/10.3390/modelling4040026>

Academic Editor: José Miguel Castro

Received: 4 September 2023

Revised: 3 October 2023

Accepted: 10 October 2023

Published: 16 October 2023



Copyright: © 2023 by the authors. Licensee MDPI, Basel, Switzerland. This article is an open access article distributed under the terms and conditions of the Creative Commons Attribution (CC BY) license (<https://creativecommons.org/licenses/by/4.0/>).

1. Introduction

Circular or Rectangular Hollow Sections (CHS or RHS) offer substantial benefits to the construction sector compared to their equivalent H-section counterparts [1–5], such as (i) high resistance against axial forces and bending moments in all directions; (ii) better performance under specific loading scenarios such as wind, water, and wave; (iii) better protection from corrosion; (iv) requires lesser volume of fire protection material; (v) easy achievement of “composite” behaviour using concrete infills (which improves the strength, stiffness and fire resistance of the member); (vi) almost 40% lighter structures; (vi) an aesthetic architectural appearance; etc. From an economic perspective, the higher price of hollow sections compared to the equivalent open sections is often compensated for in the global construction and rehabilitation process, thanks to the aforementioned benefits [2]. Therefore, hollow sections have gained some popularity in the past few decades and have been used quite frequently as column members for multi-storey structures. On the other hand, open sections are traditionally used as beam members, thus demanding a proper open-to-hollow section beam-column connection.

Currently, the most conventional ways to build a connection between an open section and a hollow section is either by directly welding the open section “branch” member (i.e.,

"I" or "H" profiles) to the hollow section "chord" wall (CHS or RHS) or by implementing external gusset plates or local stiffeners (diaphragms). In the past years, the Comité International pour le Développement et l'Etude de la Construction Tubulaire (CIDECT) has provided a significant understanding of the structural behaviour of different types of open-to-hollow section joints under various loadings, stability, fire resistance, etc. Several design guides have subsequently been developed by CIDECT for their real-life application [6–12].

Nevertheless, certain limitations have been noticed while applying these conventional open-to-CHS connections in real-life structures. Because of directly welding the I- or H-profiles to the tube wall, the CHS (or RHS) surface becomes prone to local distortions and the failure is often found to be a local yielding of the tube [13]. Furthermore, local stiffeners and gusset plates require a large amount of welding quantity and complicated fabrication works [14–17], which hinders the financial and constructional sustainability of the overall system and becomes detrimental to its aesthetic appeal. In order to avoid such issues and improve the structural performance of the open-to-hollow section connections, a "passing-through" approach was studied in several research programs [18–26] using CHS and RHS tubes. Experimental and numerical evidence proved the efficiency of the passing-through approach as local chord distortions could be avoided with reduced welding [18]. Additionally, researchers [9,20,21] stated the fact that the passing-through technique increases the RHS chord resistance by a factor of two against tensile/compressive forces. Approximately 1.65–1.96 times larger connection strength was achieved in some studies [22,23] for the passing-through connections compared to their equivalent directly-welded counterparts. Design guidelines were subsequently proposed [24] to determine the geometric and sectional properties of the pertinent parts of such a passing-through connection. Voth [25,26] also compared conventional plate-to-CHS connections with "passing through" connections under tension and compression through experiments and finite element (FE) simulations (see Figure 1), highlighting several advantages and disadvantages that can be experienced while using the passing-through technique. More recently, Di Benedetto et al. characterized the structural stiffness and failure resistance of "one-way" passing-through I-beam-to-CHS column joints using monotonic and cyclic tests as well as FE numerical studies [27,28]. A component-based design approach was subsequently proposed by the authors. Piscini A. [29] studied "four-way" steel and composite I-beam-to-CHS column connections, highlighting similar benefits in favor of the passing-through approach. A detailed state-of-the-art review can be found in [30].

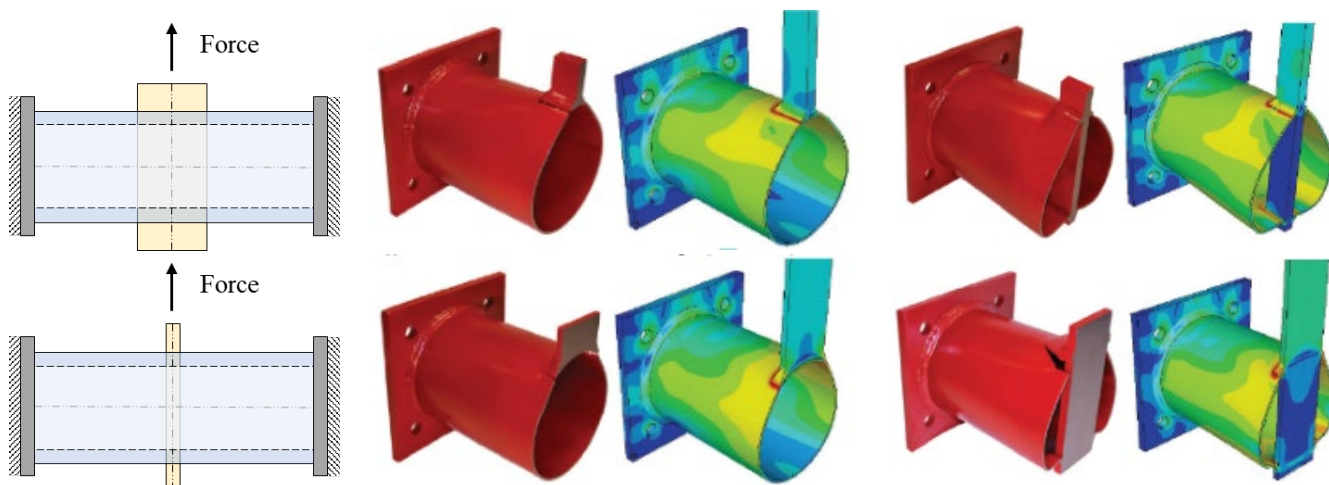


Figure 1. Different connection configurations and their failure modes studied by Voth [26].

Even though the aforementioned research investigations presented encouraging benefits of the passing-through approach, the shear and moment resisting capacity of "two-way" passing-through open-to-hollow section connections under gravitational or seismic load-

ing remain unexplored. Furthermore, practical difficulties were documented by some researchers while developing passing-through connections—firstly, the mechanical cutting of the tube slots with controlled tolerance to fit the through members, and secondly, the joint fabrication [30]. In order to solve these issues, four different two-way passing-through I-beam-to-CHS column connections were studied in an RFCS research project “LASTEICON”. Laser Cutting Technology (LCT, see Figure 2) was used to develop these connections as it offers certain advantages compared to the traditional cutting techniques—(i) increased fatigue strength [31], (ii) reduced welding due to high precision, (iii) lesser manual errors thanks to machine automation and (iv) smoother fabrication [31]. A detailed overview of the joint manufacturing or fabrication procedure can be found in [31].



Figure 2. Examples of the laser cutting process and a four-way LASTEICON joint [30].

The present article however focuses on the modelling aspects and the structural behaviour of the two types of two-way passing-through moment resisting I-beam-to-CHS column connections, so-called:

- (1) LASTEICON C3 configuration (see Figure 3a): “main” or load-carrying I-beams connected to a CHS column using an I-section passing through the tube and end-plate splices;
- (2) LASTEICON C4 configuration (see Figure 3b): “main” or load-carrying I-beams connected to the CHS column using three steel plates passing through the tube and bolted connections.

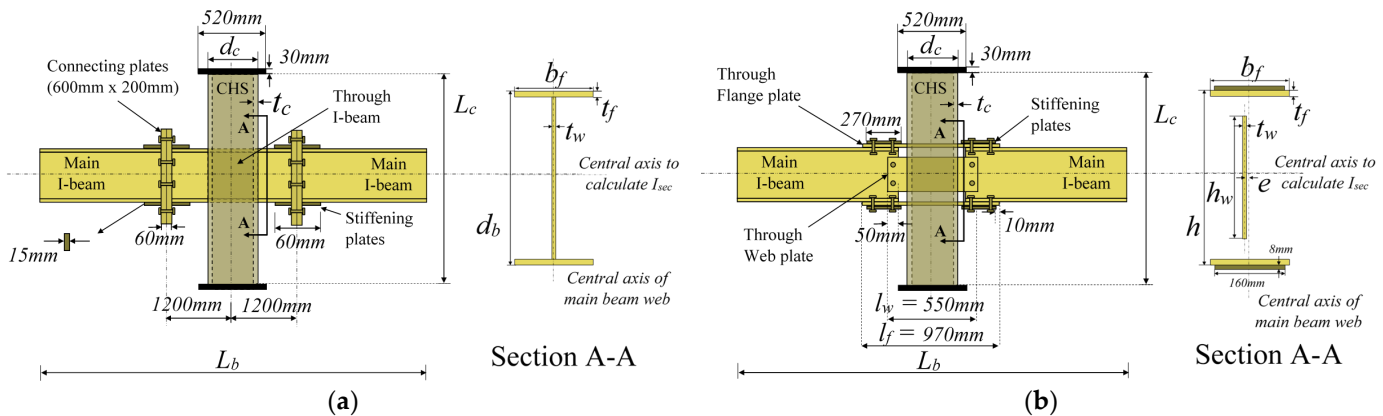


Figure 3. LASTEICON configurations (a) C3 and (b) C4.

A comprehensive experimental campaign has been conducted. Numerical finite element models have been developed. In previous publications [32,33], some preliminary comparisons have been discussed between the numerical models and a limited number of experimental tests in the context of the LASTEICON project. However, the purpose of this paper is to provide a more detailed validation of the models tentatively developed earlier, by extending them to the full set of test results available and to draw conclusions on the parameters that govern the performances of those numerical models.

2. Numerical and Experimental Investigations

2.1. Modelling Approach, Load Cases, Boundary Conditions and Material Properties

The different components of the connection configurations, such as the CHS column, passing-through I-profile, passing-through flange/web plates and the “main” beams were modelled in DIANA FEA 10.2 [34] using 3D geometries and solid elements (CTP45, CTE30, and CHX60 [34]). Uniform mesh properties were used for the CHS tube and the passing-through members for all models. The laser-cut slots were modelled to allocate the passing-through members and also to account for the possible reduction in the column stiffness. Certain assumptions were made in the FE models to avoid secondary connection failures, save computation time, avoid convergence issues and put major emphasis on the passing-through zone: (i) the slots were assumed to have no tolerance, hence perfectly fitting the through members with the CHS column, and (ii) bolts and welds (as shown in Figure 3) were in purpose designed to have an overstrength in the experiments, therefore not constituting any possible weak point of the system. As a consequence, they are not modelled explicitly, but only as perfect contact points. Figure 4 illustrates some examples of the FE models.

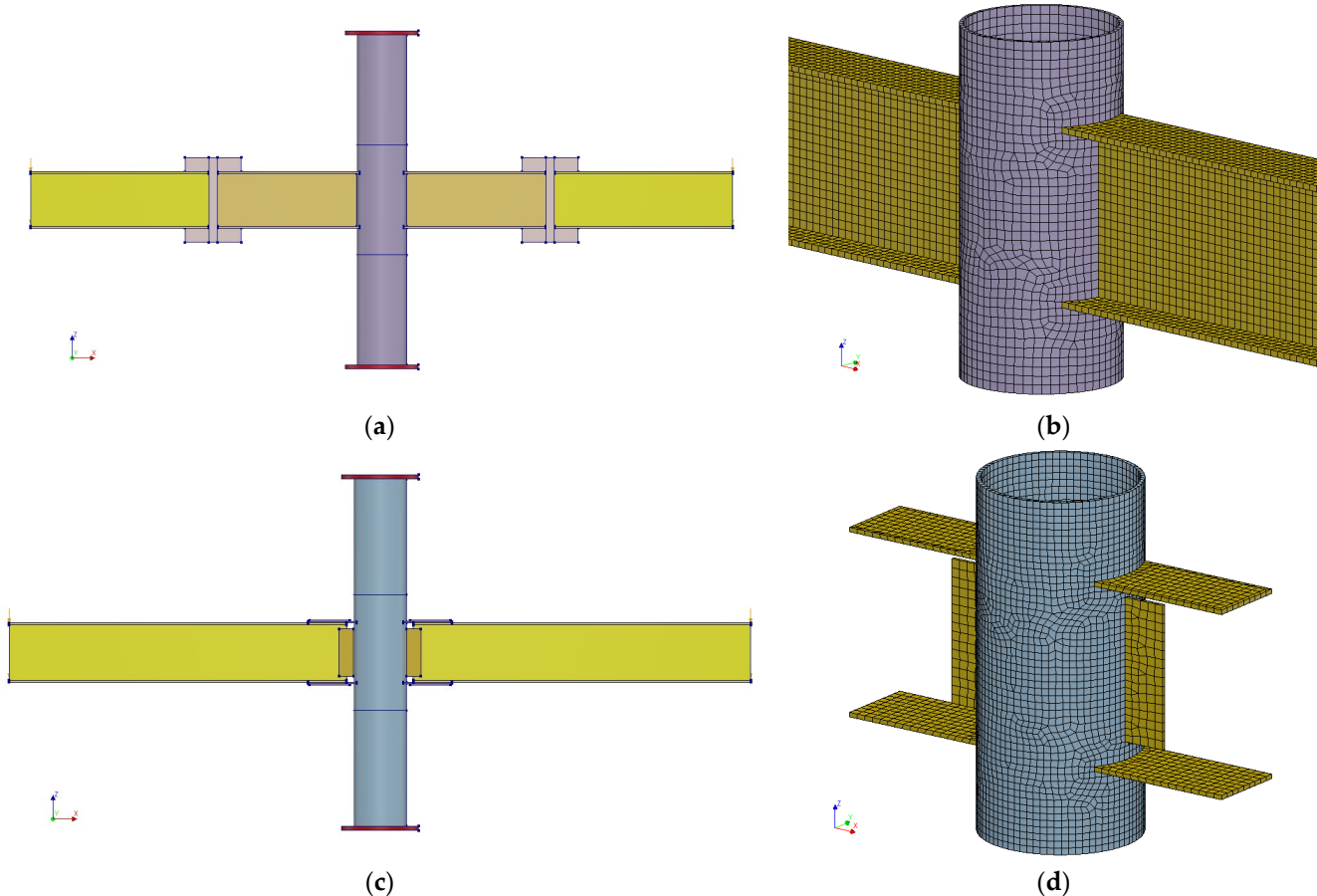


Figure 4. Finite element (FE) models developed in DIANA FEA 10.2, (a) front view of configuration C3, (b) meshed passing-through connection zone for C3, (c) front view of configuration C4, and (d) meshed passing-through connection zone for C4.

The configurations were investigated under two different types of loading—a gravitational loading, LC1 (Figure 5a) and an opposite bending loading, LC2 (Figure 5b). The loads were applied at the free ends of the main beams and were incremented simultaneously until failure. “Failure” in the FE models was identified by comparing the accumulated plastic strains in the model to an experimentally calibrated “limit”. Pinned support conditions

were used at both ends of the CHS column. Lateral supports were provided at the flange corners of both ends of the main beams.

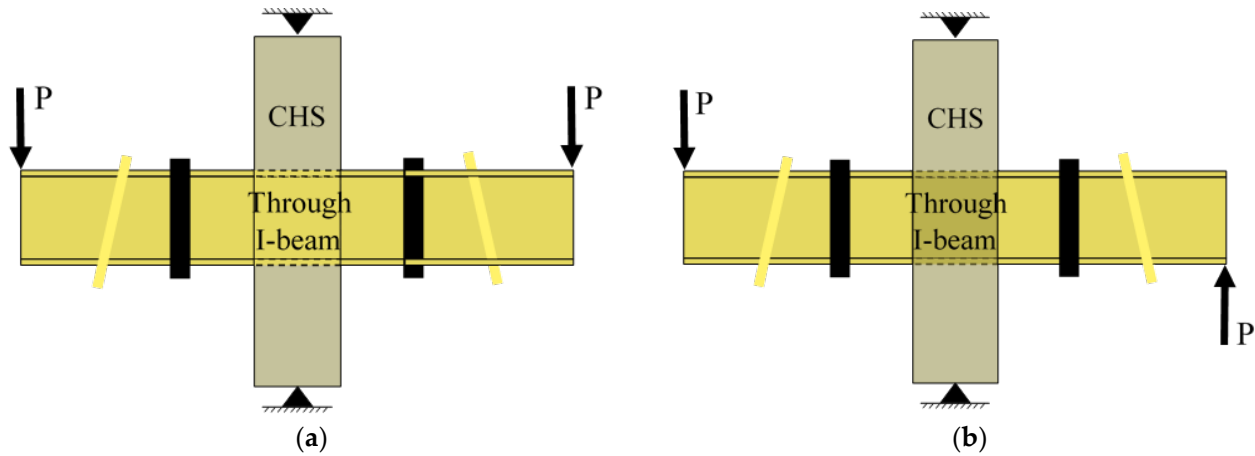


Figure 5. (a) Gravitational loading, LC1 and (b) opposite bending loading, LC2.

Geometric and material nonlinearities were considered in the numerical simulations. The material stress-strain properties for each component were obtained from the coupon tests, which were later converted into real stress-strain curves (see Figure 6) and used in the finite element (FE) models. Although the different structural components of each configuration were pre-designed with an S355 steel grade, five different material yield strengths were obtained as shown in Figure 6. The material yield strengths for the 8 mm thick plates (P8), 10 mm thick plates (P10), 12 mm thick plates (P12), I-beam sections and the CHS columns were obtained as 350 MPa, 300 MPa, 420 MPa, 355 MPa and 377 MPa respectively. Relevant material properties were used with respect to each specimen and its components to compare the FE models with the test results.

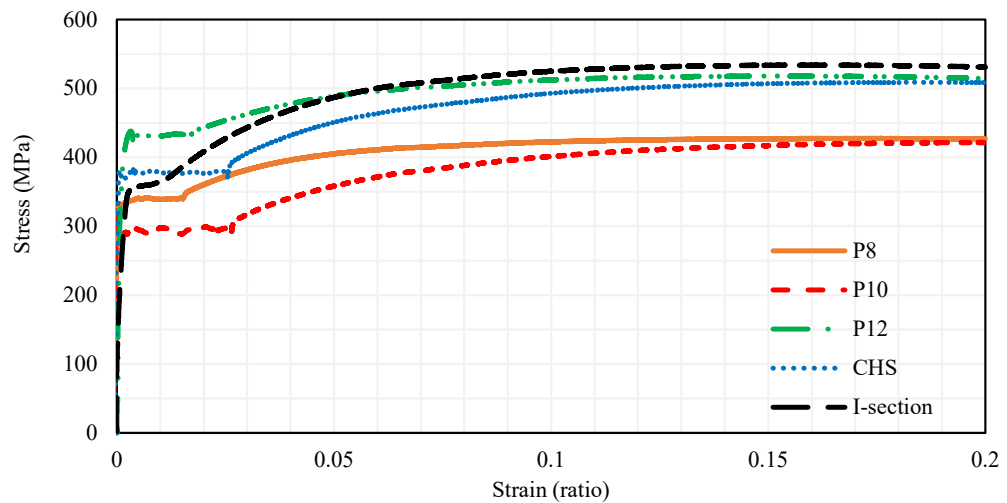


Figure 6. Material stress-strain relationships obtained from the experimental tests.

2.2. Experimental Test Set-Up and Load Application

Experiments were carried out at INSA Rennes. 520 mm × 30 mm solid circular plates were welded to both ends of the CHS (see Figure 7) in order to provide rollers as per the required support conditions shown in Figure 5.

The testing frame consisted of a HEB 400 beam connected to two HEA 300 columns, with four HEA 200 sections acting as lateral bracings (Figure 7). The roller at the bottom of the CHS was supported by the testing floor while the upper one was supported by the

HEB 400 beam of the testing frame. Stiffeners were welded to the I-beam flanges in C3 and flange plates in C4 at the connection zones between the through members and the “main” beam to avoid any localised buckling. Such additional components are duly considered in the models to have a straightforward and consistent comparison between the numerical and experimental outcomes. Two jacks with a maximum capacity of 1500 KN, were used to apply the vertical loads at the free ends of the main beam (denoted by red arrows in Figure 7) at 2500 mm distance from the central axis of the tube for LC1. A reduced distance of 1700 mm was adopted for LC2 in order to have a sufficient margin for larger rotations of the node at failure. The length of the CHS column was taken as 2340 mm in all cases. The “main” beams were chosen as IPE 400 in all cases. LVDTs and inclinometers were located at relevant places. Complete details regarding the experimental campaign can be found in [35,36].

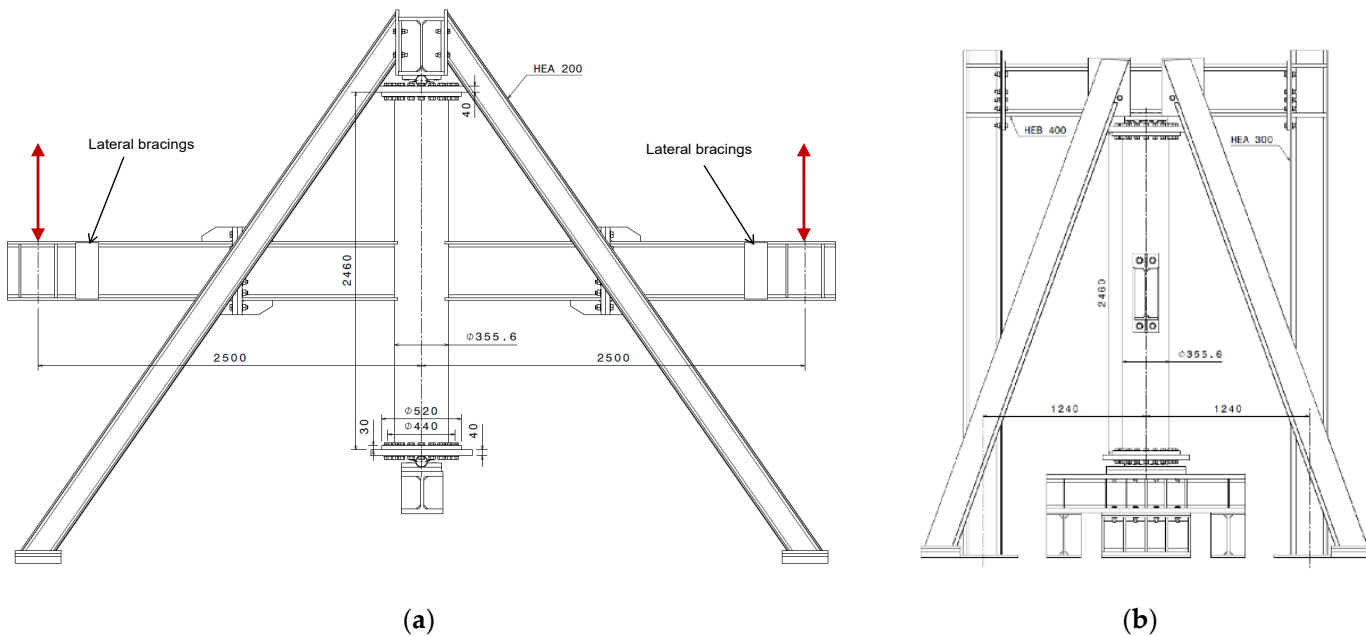


Figure 7. Description of the test set-up used at INSA; Rennes (a) front view and (b) side view [36].

2.3. Description of the Investigated Connections

2.3.1. Configuration C3

Six tests were conducted on the LASTEICON C3 configuration. A complementary investigation was also conducted on a conventional I-beam-to-CHS connection configuration, namely CoC3, under LC1 without any passing-through I-beam. In this case, the I-beams were directly welded to the tube. Relevant geometric and section properties of all the tested specimens corresponding to C3 are listed in Table 1. All experiments were utilized to calibrate the numerical models. The numerically obtained force–displacement behaviour and failure modes were compared with the test results. A good ductile behaviour was achieved for the C3_LC1 and CoC3_LC1 specimens. Therefore, once the maximum joint strength was achieved, the load application was stopped at an arbitrary point. On the contrary, the test results from C3_LC2 showcased a less ductile behaviour as the failure was governed by the CHS wall tearing near its welded connection with the passing-through I-beam flange.

Table 1. LASTEICON C3 experiments used for numerical calibration.

Config. Type	Load Case	Test No.	Specimen Name	Through Beam	CHS Dimensions		Welding Type
					d_c (mm)	t_c (mm)	
LASTEICON C3	LC1	1	C3-1	IPE 400	355.6	08.8	Full penetration
	LC1	2	C3-2	IPE 400	355.6	10.0	Fillet
	LC1	3	C3-3	IPE 400	355.6	12.5	Fillet
	LC2	4	C3-2	IPE 400	355.6	10.0	Fillet
	LC2	5	C3-3	IPE 400	355.6	12.5	Fillet
	LC2	6	C3-1	IPE 400	355.6	08.8	Full penetration
Conventional CoC3	LC1	7	C3-0	IPE 400	355.6	10.0	N.A.

2.3.2. Configuration C4

Similarly, six tests were conducted on the LASTEICON C4 configuration. A single investigation was conducted on a conventional configuration, namely CoC4, under LC1, where the flange and web plates were directly welded to the tube. Table 2 shows the relevant geometric and section properties of all the tested specimens corresponding to C4. The experiments regarding C4_LC1 were characterized by a brittle behaviour through flange plate buckling under compressive forces. The tests were, however, extended further, even after reaching the brittle failure mode, to observe the post-peak behaviour of such a joint configuration. Finally, the tests were stopped at an arbitrary point when a consistent fall was noticed in the load–displacement behaviour. However, the C4_LC2 and CoC4_LC1 specimens failed in a similar way to C3_LC2. The failure was governed by the tube wall tearing near its welded connection between the through flange plates under tension. It is relevant to note that some bolts sliding was observed in the C4 joints under LC1 so the total vertical displacement of the whole system was affected. However, as the bolts were not modelled explicitly in the numerical models to avoid any unnecessary complication due to the secondary connections, such sliding behaviour was not obtained from the numerical simulations. Thus, in order to obtain reliable validation, the experimental force–displacement curves under LC1 were thoroughly investigated and were further refined by eliminating the relative sliding of the bolts, which could be obtained from the relevant strain gauges [33,35]. The modified force–displacement curves were then compared with the numerical results.

Table 2. LASTEICON C4 experiments used for numerical calibration.

Config. Type	Load Case	Test No.	Specimen Name	Through Plate(s) Dimensions					d_c (mm)	t_c (mm)	Welding Type
				h (mm)	b (mm)	h_w (mm)	t_w (mm)	t_f (mm)			
LASTEICON C4	LC1	8	C4-4	424	180	320	10.0	12.0	355.6	10.0	Full penetration
	LC1	9	C4-1	424	180	320	08.0	10.0	355.6	08.8	Full penetration
	LC1	10	C4-5	424	180	320	08.0	10.0	355.6	12.5	Fillet
	LC2	11	C4-6	424	180	320	10.0	12.0	355.6	12.5	Fillet
	LC2	12	C4-2	424	180	320	10.0	12.0	355.6	08.8	Full penetration
	LC2	13	C4-4	424	180	320	10.0	12.0	355.6	10.0	Full penetration
Conventional CoC4	LC1	14	C4-0	424	180	320	08.0	10.0	355.6	8.8	N.A.

3. Results and Discussions

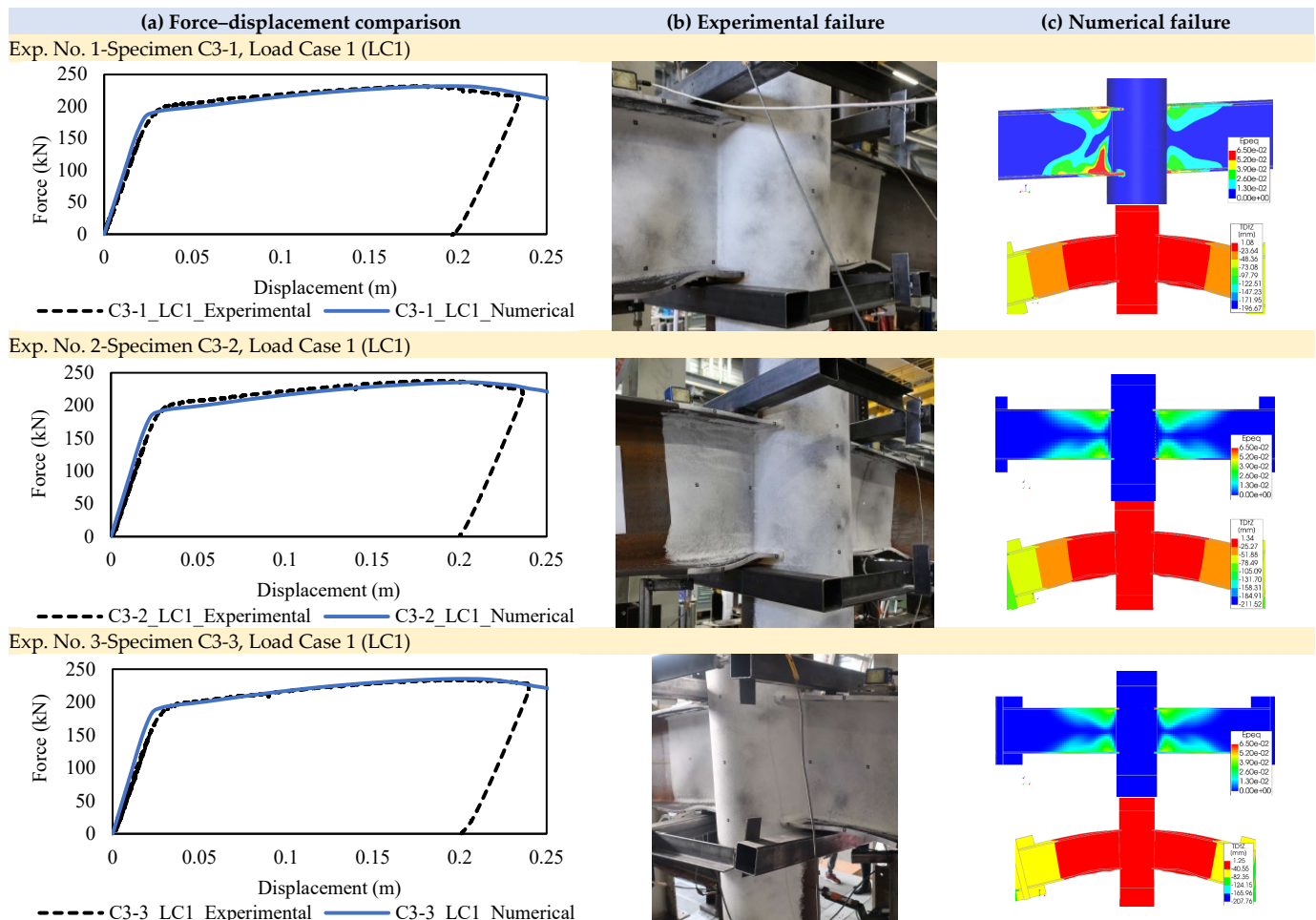
3.1. Configuration C3

This section compares the experimental and numerical force–displacement behaviour of LASTEICON Configuration C3. The failure modes are also compared and characterised.

Finally, the behaviour of the LASTEICON C3 configuration is compared with the conventional directly welded connection configuration (CoC3) to highlight the benefits of the passing-through approach.

3.1.1. LC1: Monotonic Gravitational Loading

The experimental and numerical force–displacement curves are compared for all C3 specimens under LC1 as shown in Figure 8a. Both the joint strength and stiffness were observed to be approximately the same. Identical failure modes were obtained from the FE models and their corresponding experimental specimens as shown in Figure 8b,c. The failure due to the yielding of the I-beam flange can be clearly noticed for all the C3 specimens just outside the CHS, where the deformed flanges of the tested specimen correspond to the concentrated high strain values obtained from the FE models at a similar location of the through-beam flanges, as shown in Figure 8b,c respectively. The vertical loads applied at the free end of the main beams create moments at both sides of the joint, which activates the passing-through I-beam flanges under tension-compression couples. However, due to the fact that the passing-through I-beam web provides anchorage to its flanges, the joint panel behaves as a rigid body. As a result, the moments do not locally affect the I-beam flanges and instead shift outside the CHS, where the I-section fails in flexure. No localised distortions or damages in the CHS column wall were noticed in these cases. As the bending resistance of the through I-beam alone determined the failure of such joints under LC1, different welding techniques (FS fillet welding or full-penetration welding) did not have any influence on the connection behaviour.



3.1.2. LC2: Monotonic Opposite Bending Loading

Figure 9a showcases a good agreement between the numerical and experimental joint strength and stiffness under LC2 for the specimens having FS fillet welds. A different force-transfer mechanism was noticed under such an opposite bending load case. The moment produced at the joint due to the antisymmetrical loads at the main beams' extremities is resisted by a combined effort of two components: (i) the transverse shear resistance of the web inside the CHS and (ii) the transverse axial resistance of the tube wall. The ultimate failure in the C3-2_LC2 specimens was visualized as a CHS column wall tearing at the connection zone between the CHS column and the passing-through flanges (Figure 9b). Such a similar failure behaviour was obtained from the numerical models as ultimate stresses and limiting plastic strains developed around the connection zone as shown in Figure 9c, thus providing suitable validation to the numerical models. It is also important to state that the shear stresses in the passing-through I-beam web were observed to distribute in a uniform manner along the height of the web, thanks to the anchorage provided by the I-beam flanges—which was not the case for the C4 configuration, as discussed later. Nevertheless, for the C3_LC2 specimen (Exp. No. 6) with full penetration welding, although similar failure modes were attained from the numerical simulations with respect to the experimental prototypes, the joint strength and stiffness values did not have a perfect match. The experimental values were much lower compared to the numerical results. This occurred due to the full-penetration type of welding used to connect the through I-beam to the CHS column. As the CHS column wall is subjected to additional cutting and heating for such a welding technique, the local properties of the CHS wall might be adversely affected, i.e., reducing its transverse tensile/compressive capacity, which then leads to a reduction in the overall joint strength. As the weld itself was not explicitly considered in these global numerical models, such a phenomenon could not be predicted by the FE simulations at this stage. However, this is noted to be a crucial point and is currently being investigated with detailed models of the welded zone in the frame of another European research project “LASTTS” [37]. In this piece of research, three different types of welding have been considered to connect the passing-through member with the CHS column, i.e., (i) full-penetration butt welds, (ii) full-strength fillet welds and (iii) partial strength fillet welds. This project contemplates experimental tests and numerical parametric studies. The preliminary results showcase no strength degradation when full-penetration welds are used, which hints towards the fact that the full-penetration welded connections considered in the present paper were possibly not adequately designed or executed. Detailed results regarding the welding types can be found in [38]. Furthermore, it is also interesting to mention that this new research project LASTTS also investigates the effects of laser cutting for mild steel grades S235–S460 subjected to high-cycle fatigue loadings to characterize the heat-affected zones [39].

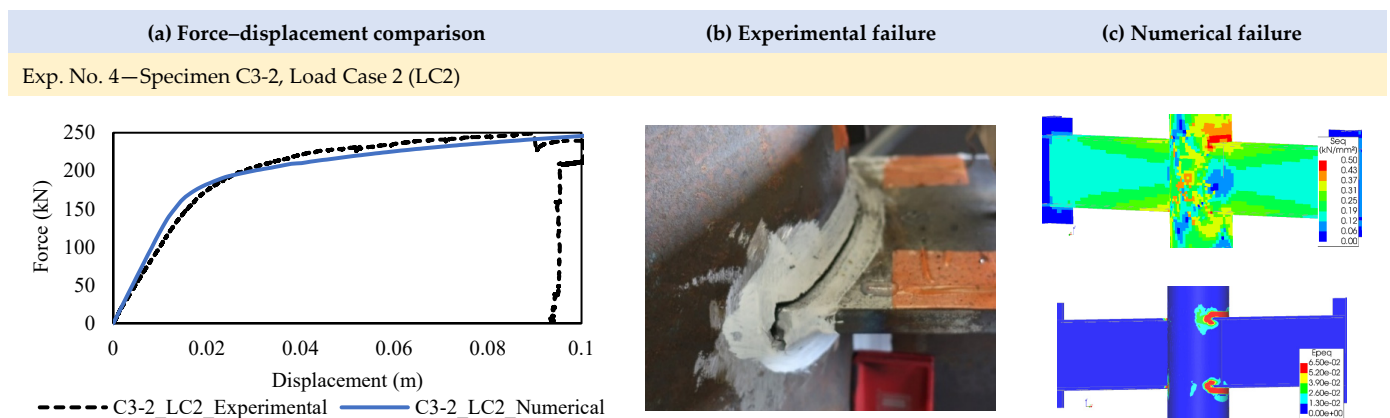


Figure 9. Cont.

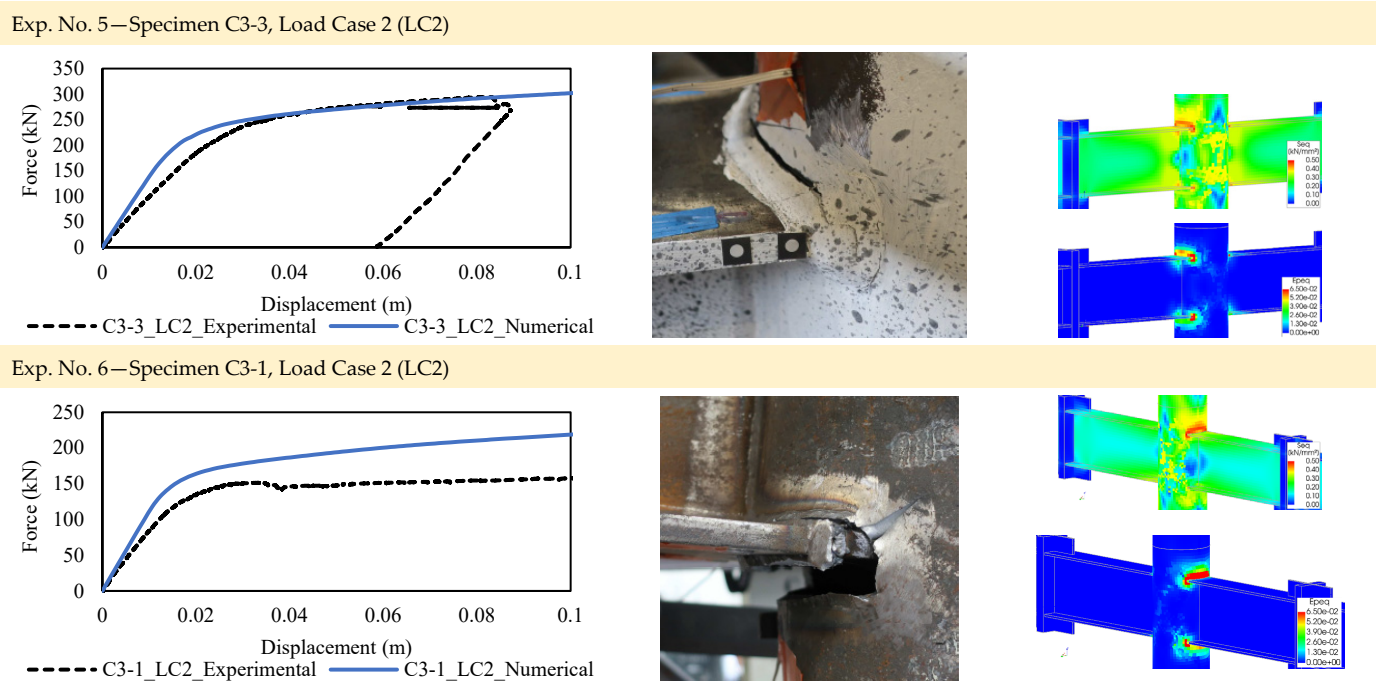


Figure 9. Comparison of experimental and numerical results through force–displacement curves, experimental and numerical failure modes for Configuration C3 specimens under LC2 [32,36].

3.1.3. Comparison with a Conventional Connection, CoC3

The experimental and numerical force–displacement curves for the only conventional joint configuration, CoC3, under LC1, are compared in Figure 10a to show the good agreement obtained in terms of joint strength and stiffness. Similar results were also obtained regarding the failure mode, i.e., tube wall crushing under compression (see Figure 10b) denoted by the concentrated plastic strains (Figure 10c) at the connection zones.

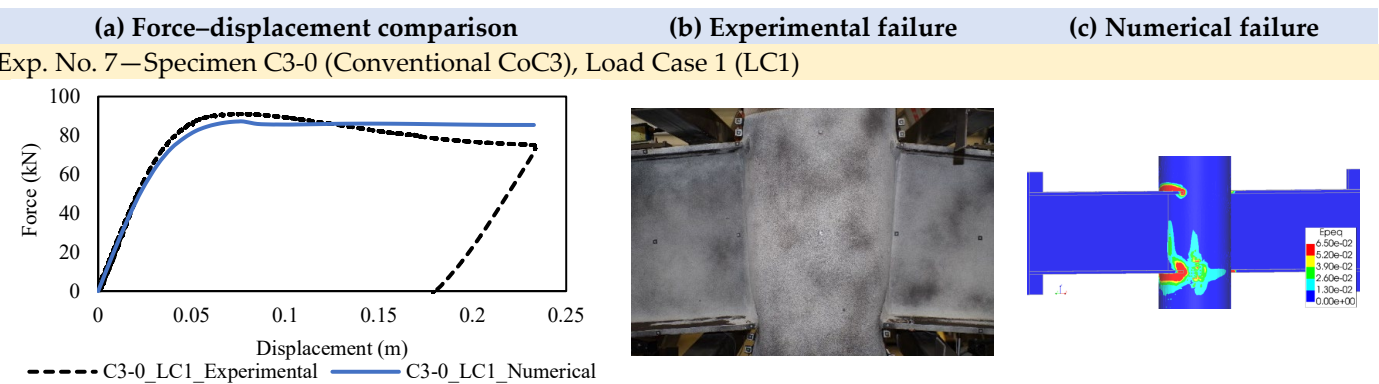


Figure 10. Comparison of experimental and numerical results through force–displacement curves, experimental and numerical failure modes for Configuration CoC3 specimen under LC1 [32,36].

A comparison between the LASTEICON C3 configuration and the directly welded CoC3 configuration under LC1 highlights the advantages of the passing-through approach. Two tested specimens with the same sectional properties for the primary members, i.e., the main beams and the column (IPE 400 and CHS 355.6 × 10.0 respectively) can be compared (i.e., Exp. No. 2 for C3 and Exp. No. 7 for CoC3) as listed in Table 1. A significant difference is observed in the joint strength and stiffness. Thanks to the added contribution offered by the passing-through member, the proposed technique produces approximately 2.5 times higher strength and 10 times higher stiffness compared to a conventional directly welded technique.

3.2. Configuration C4

This section compares the experimental and numerical force–displacement behaviour of LASTEICON Configuration C4. The failure modes are subsequently compared and characterised. Furthermore, the behaviour of the LASTEICON C4 configuration is compared with the conventional directly welded connection configuration (CoC4).

3.2.1. LC1: Monotonic Gravitational Loading

As shown in Figure 11a, the numerical force–displacement behaviour of the LASTEICON C4 joints had a good agreement with the experimental joint strength and stiffness. The behaviour of the C4 joints was observed to be different compared to the C3 joints. The vertical loads applied at the free end of the main beams create moments at both sides of the joint, which in turn create tension-compression couples at the passing-through flange plates. Unlike the C3 joints, the inserted web plate in C4 does not have a direct connection with the flange plates and therefore fails to provide any anchorage. The tension-compression couples therefore act essentially on the flange plates, making them vulnerable towards buckling under compression. The internal diameter of the CHS column, in this case, determines the effective buckling length of the compressed plate. Finally, the failure in all the C4_LC1 specimens is governed by the buckling resistance of the through flange plate (Figure 11b) inside the CHS—corresponding to the peak values in Figure 11. After the buckling failure of the flange plate, the web plate takes up the compressive forces and also eventually fails due to buckling inside the CHS. Finally, a stable quasi-horizontal plateau with a descending behaviour is noticed.

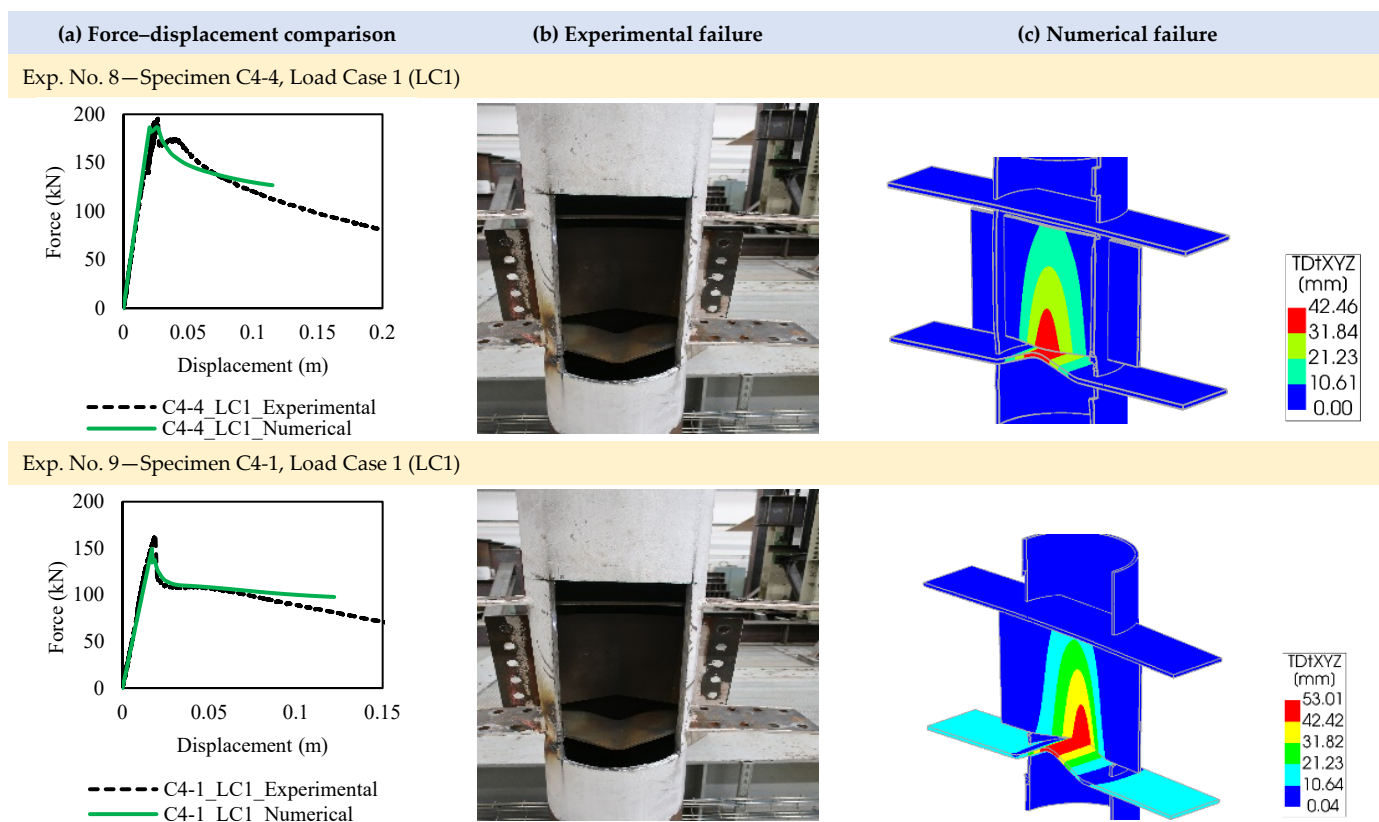


Figure 11. Cont.



Figure 11. Comparison of experimental and numerical results through force–displacement curves, experimental and numerical failure modes for Configuration C4 specimens under LC1 [33,35].

The FE models failed in an identical manner as the experimental prototypes. Concentrated deformations (Figure 11c) and plastic strains obtained from the FE models on the inserted part of the passing-through plates clearly replicate the flange and web plate buckling obtained from the experiments. No localised distortions or damages in the CHS column wall were noticed in these cases. As the buckling resistance of the passing-through flange plate inside the CHS determines the failure mechanism of such a joint, the different welding techniques (FS fillet welding or full-penetration welding) did not have any influence on the connection behaviour. An unexpected increase was however obtained in the experimental joint strength in Exp. No. 10. This occurred as the bottom flange plate buckled upwards and came in contact with the web plate, thus providing additional strength to the web plate. However, because (i) the flange plate buckling is considered to be the primary failure mode for the C4 configuration under LC1 and (ii) a gain in strength due to the unpredictable contact between the flange and web plates cannot be considered during design calculations, contact elements and a specified imperfection (i.e., forcing an upward buckling of the flange plates) were not used in the numerical models to predict such a phenomenon. This can be stated as a limitation of the current modelling approach and has been perceived as a topic for future research.

3.2.2. LC2: Monotonic Opposite Bending Loading

Figure 12a shows the good agreement obtained between the numerical and experimental force–displacement curves for the LASTEICON C4 specimen, with fillet welds, under LC2. Similarly, to the C3 configuration, a different force transfer mechanism was noticed in the C4 configuration under LC2. The joint resistance is achieved through 2 components: (i) the transverse shear resistance of the passing-through web plate and (ii) the transverse axial resistance of the CHS. Failure in the tested specimens occurred due to the CHS wall tearing at the through flange plate-to-CHS welded connection (Figure 12b). High strain concentrations were obtained in the FE models at the same locations. However, due to the discontinuity between the passing-through flange and web plates in Configuration C4, the shear stress distribution in the passing-through web plate was observed to be more parabolic than rectangular—which was the case for Configuration C3—which therefore slightly reduces the joint resistance for such connections compared to the previous one.

Due to the same reason stated in Section 3.1.2, a perfect agreement was not obtained for the C4 specimens with full-penetration welding (Exp. No. 12 and 13) under LC2. A comparatively lower joint strength with a more progressive degradation of the stiffness was observed from the experiments. As the welds or heat-affected zones (HAZ) were not explicitly modelled in this study, such a phenomenon could not be predicted by the FE simulations at this stage and is currently being investigated in the frame of another European research project “LASTTS” [37].

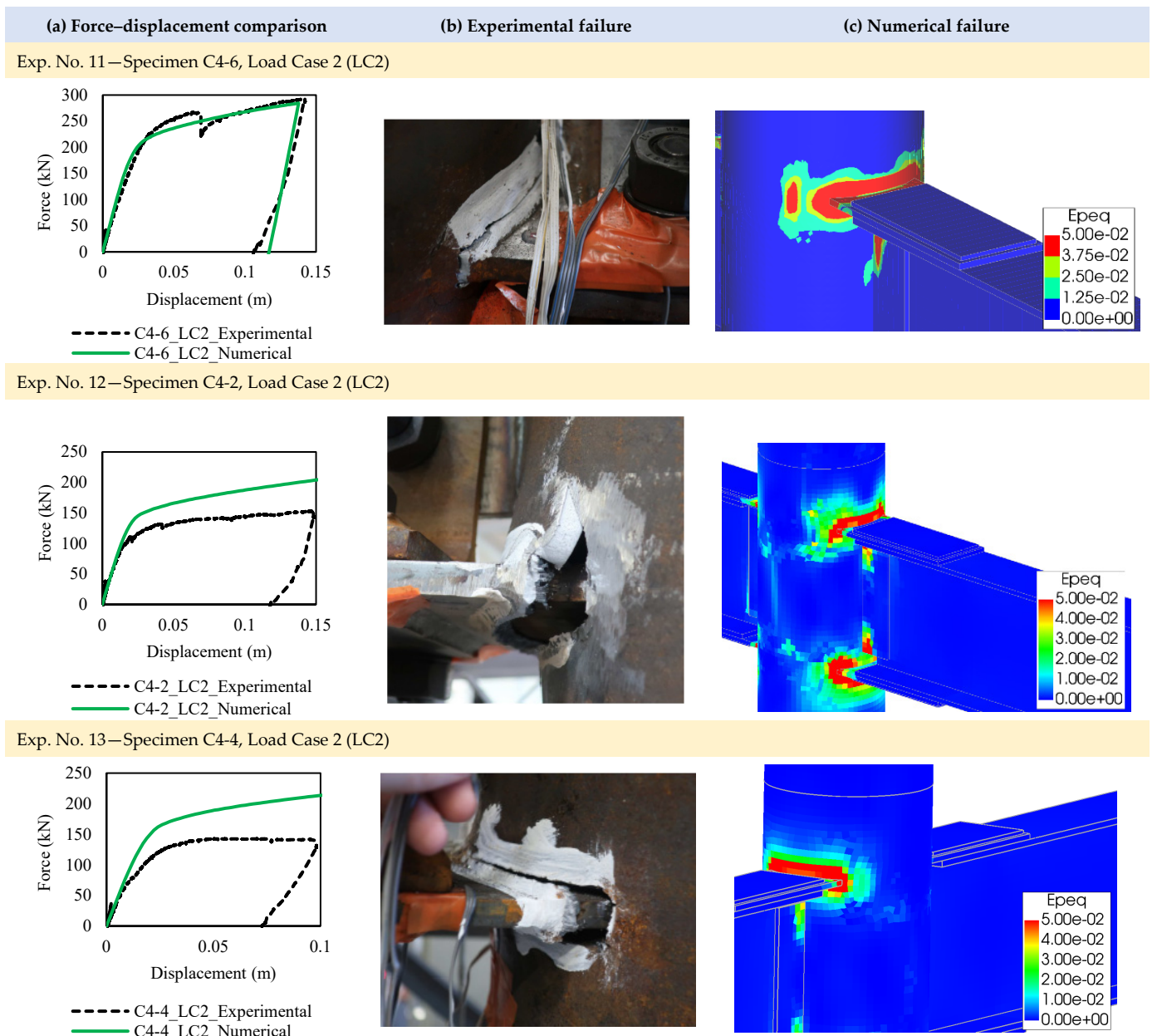


Figure 12. Comparison of experimental and numerical results through force–displacement curves, experimental and numerical failure modes for Configuration C4 specimens under LC2 [33,35].

3.2.3. Comparison with a Conventional Connection, CoC4

The experimental and numerical force–displacement curves for the corresponding conventional joint configuration, CoC4, under LC1, are compared in Figure 13a to showcase the good agreement obtained in terms of joint strength and stiffness. Similar results were also obtained regarding the failure mode. During the tests, the CHS wall was crushed under compression (Figure 13b) at the connection zones. Concentrated high-strain values were identified at the same location (Figure 13c) from the FE models.

Similar to the C3 configuration, a comparison study was conducted between the LASTEICON C4 specimen (Exp. No. 9) and the directly welded CoC4 specimen (Exp. No. 14) under LC1, which had the same sectional properties for the main I-beams (IPE400), flange plates, web plates and the CHS column (355.6×8.8), as listed in Table 2. The passing-through C4 specimen produced an approximately 2 times higher strength and 10 times higher stiffness compared to the conventional CoC4 specimen.

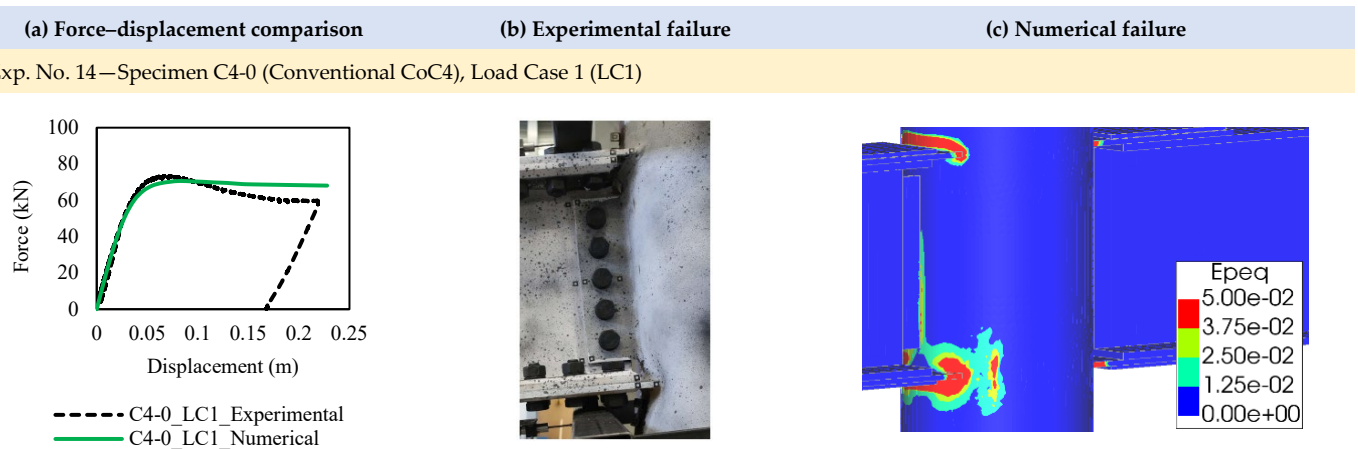


Figure 13. Comparison of experimental and numerical results through force–displacement curves, experimental and numerical failure modes for Configuration CoC4 specimens under LC1 [33,35].

4. Conclusions

This article presents the finite element (FE) modelling of two types of innovative passing-through I-beam-to-CHS column connections realised with laser cutting technology (LCT). The FE modelling approach essentially consists of three stages: (i) model development based on experimental data i.e., the material stress–strain curves, boundary conditions, different loading scenarios, etc. (ii) calibration against experimentally obtained failure strains and (iii) validation in terms of the force–displacement behaviour and failure modes obtained from the tested specimens. Relevant modelling assumptions, numerical results and experimental references are discussed in the article to provide a clear view of the structural behaviour of the laser-cut connections.

Under monotonic gravitational loading (LC1), a good agreement is obtained for all tested specimens (irrespective of the welding type) between the experimental and numerical force–displacement behaviours (joint strength and stiffness) and failure modes. Under opposite bending loads (LC2), even though the failure occurred at the connection zones between the passing-through members and the CHS column, an equally good agreement is achieved for the joint specimens having fillet weld connections. Furthermore, not considering explicitly the bolted connections in the FE models do not have any adverse effect on the numerical predictions. Therefore, based on the overall results, the FE modelling approach has been deemed suitable for further parametric studies and the eventual development of standard design guidelines [32,33]. However, two main limitations are addressed: (i) explicit modelling of the full-penetration welds between the passing-through members and the CHS column is necessary to further validate the numerical models and identify the reason behind the strength degradation observed for the corresponding case studies and (ii) contact surfaces and a specific initial imperfection (to force an upward buckling of the flange plate in C4) can provide a better post-peak prediction, although not necessary from a design perspective as they can lead to overcomplicated models with non-convergence issues and reduced time-efficiency. Further investigations on the first of those limitations is currently being considered as a main point in an ongoing European research project “LASTTS” [37], which deals with a similar type of laser-cut joints.

The structural performance of the LASTEICON joints was also investigated and compared with each other to highlight their benefits and limitations. Passing-through I-beams offer a greater resistance and avoid a brittle plate buckling failure compared to passing-through plates with approximately equal amounts of steel. However, passing-through plates offer easy fabrication and a simpler way to construct four-way joints, which can often prove to be cost-effective. Furthermore, the passing-through joints provide approximately 2.0–2.5 times the joint strength and 9.0–10.0 times the joint stiffness compared

to a conventional directly welded I-beam-to-CHS column connection with similar section properties for the main beam and the CHS column.

Author Contributions: All authors contributed to the study's conception and design. Material preparation, numerical modelling, linear and nonlinear simulations and post-processing results were performed by R.D. Checking the results, interpreting them, and reviewing the article were carried out by A.K. and H.D. The first draft of the manuscript was written by R.D. Supervision and provision of resources were carried out by A.K. and H.D. All authors have read and agreed to the published version of the manuscript.

Funding: This project has received funding from the European Union, Research Fund for Coal and Steel under grant agreement No 709807. Views and opinions expressed are however those of the author(s) only and do not necessarily reflect those of the European Union or Research Fund for Coal and Steel. Neither the European Union nor the Research Fund for Coal and Steel can be held responsible for them.

Data Availability Statement: The authors confirm that the data supporting the findings of this study are available within the article. Requests for any additional data may be made through the corresponding author.

Acknowledgments: This research study was possible thanks to the research fund provided by the European Commission with the contract LASTEICON EU-RFCS GA-709807 "www.LASTEICON.eu" (accessed on 3 September 2023)". The authors express their immense gratitude towards Mael Couchaux, Department of Civil and Urban Engineering, National Institute of Applied Sciences of Rennes, France, for granting the availability of the experimental results. The project consortium also includes Fincon Consulting Italia srl (coordinator), RWTH Aachen, University of Pisa, Hasselt University, Instituto Superior Tecnico of Lisbon and INSA Rennes, ADIGESYS, OCAM and VALLOUREC. The cooperation of all of them is hereby gratefully acknowledged.

Conflicts of Interest: The authors declare no conflict of interest.

References

1. Wardenier, J.; Packer, J.A.; Zhao, X.L.; Van der Vegte, G.J. *Hollow Sections in Structural Applications*; CIDECT: Geneva, Switzerland, 2010.
2. Wardenier, J.; Kurobane, Y.; Packer, J.A.; Van der Vegte, G.J.; Zhao, X.L. *Design Guide for Circular Hollow Section (CHS) Joints under Predominantly Static Loading*; CIDECT Design Guide 1; LSS Verlag: Dortmund, Germany, 2008.
3. Bursi, O.S.; Ferrario, F.; Haller, M.; Lennon, T.; Bianco, L.; Mallardo, R.; Demonceau, J.-F.; Franssen, J.-M.; Jaspart, J.-P.; Hanus, F.; et al. *Prefabricated Composite Beam-to-Column Filled Tube or Partially Reinforced-Concrete Encased Column Connections for Severe Seismic and Fire Loadings*; RFSR-CT-2003-00034, Final Report; European Commission: Brussels, Luxembourg, 2009.
4. Demonceau, J.F.; Hoang, V.L.; Jaspart, J.P. *Performance-Based Approaches for High Strength Tubular Columns and Connections under Earthquake and Fire Loadings*; RFSR CT-2008-00037, Final Report; European Commission: Brussels, Luxembourg, 2013.
5. BLM Group. *All in One Tube Technology No: 20, Inspired Tube*; BLM Group: Ampthill, UK, 2015; Available online: <https://www.blmgroup.com/all-in-one> (accessed on 3 September 2023).
6. De Winkel, G.D.; Puthli, R.S.; van Foeken, R.; Lu, L.H.; Rink, H.D.; Verheul, A.; Wardenier, J. *Semi-Rigid Connections between I-Beams and Tubular Columns*; Final Report, ECSC-EC-EAEC; European Commission: Brussels, Luxembourg, 1995.
7. Rondal, J.; Würker, K.G.; Dutta, D.; Wardenier, J.; Yeomans, N. *Structural Stability of Hollow Sections*; CIDECT Design Guide 2; Verlag TÜV Rheinland: Cologne, Germany, 1992.
8. Dutta, D.; Wardenier, J.; Yeomans, N.; Sakae, K.; Bucak, O.; Packer, J.A. *Design Guide for Fabrication, Assembly and Erection of Hollow Section Structures*; CIDECT Design Guide 7; Verlag TÜV Rheinland: Cologne, Germany, 1998.
9. Kurobane, Y.; Packer, J.A.; Wardenier, J.; Yeomans, N. *Design Guide for Structural Hollow Section Column Connections*; CIDECT Design Guide 9; Verlag TÜV Rheinland: Cologne, Germany, 2004.
10. Packer, J.A.; Sherman, D.R.; Lecce, M. *Hollow Structural Section Connections*; Steel Design Guide 24, Steel Design Guide Series; American Institute of Steel Construction: Chicago, IL, USA, 2010.
11. Jaspart, J.P.; Weynand, K. Design of hollow section joints using the component method. In *Tubular Structures XV, Proceedings of the 15th International Symposium of Tubular Structures (ISTS), Rio de Janeiro, Brazil, 27–29 May 2015*; CRC Press: Boca Raton, FL, USA, 2015; pp. 405–410.
12. Jaspart, J.P.; Pietrapertosa, C.; Weynand, K.; Busse, E.; Klinkhamer, R.; Grimault, J.P. *Development of a Full Consistent Design Approach for Bolted and Welded Joints in Building Frames and Trusses between Steel Members Made of Hollow and/or Open Sections—Application of the Component Method, Volume 1—Practical Guidelines*; CIDECT Report: 5BP-4/05; CIDECT: Aachen, Liege, 2005.
13. Alostaz, Y.M.; Schneider, S.P. *Connections to Concrete-Filled Steel Tubes*; A Report on Research Sponsored by the National Science Foundation NSF CMS 93-00682; University of Illinois Urbana-Champaign: Champaign, IL, USA, 1996.

14. Fukumoto, T.; Morita, K. Elastoplastic behavior of panel zone in steel beam-to-concrete filled steel tube column moment connections. *ASCE J. Struct. Eng.* **2005**, *131*, 1841–1853. [[CrossRef](#)]
15. Nishiyama, I.; Fujimoto, T.; Fukumoto, T.; Yoshioka, K. Inelastic force-deformation response of joint shear panels in beam-column moment connections to concrete-filled tubes. *ASCE J. Struct. Eng.* **2004**, *130*, 244–252. [[CrossRef](#)]
16. Morino, S.; Tsuda, K. Design and construction of concrete-filled steel tube column system in Japan. *Earthq. Eng. Eng. Seismol.* **2002**, *4*, 51–73.
17. Fujimoto, T.; Inai, E.; Kai, M.; Mori, K.; Mori, O.; Nishiyama, I. Behavior of beam-to-column connection of CFT column system. In Proceedings of the 12th World Conference on Earthquake Engineering, Auckland, New Zealand, 30 January–4 February 2000; pp. 1–8.
18. Alostaz, Y.M.; Schneider, S.P. Analytical behavior of connections to concrete-filled steel tubes. *J. Constr. Steel Res.* **1996**, *40*, 95–127. [[CrossRef](#)]
19. Kosteski, N.; Packer, J.A. Experimental examination of branch plate-to-RHS member connection types. In Proceedings of the 9th International Symposium of Tubular Structures, Dusseldorf, Germany, 3–5 April 2001; pp. 135–144.
20. Kosteski, N.; Packer, J.A. Longitudinal plate and through plate-to-hollow structural section welded connections. *ASCE J. Struct. Eng.* **2003**, *129*, 478–486. [[CrossRef](#)]
21. Kosteski, N. Branch Plate to Rectangular Hollow Section Connections. Ph.D. Thesis, University of Toronto, Toronto, ON, Canada, 2001.
22. Willibald, S.; Packer, J.A.; Voth, A.P.; Zhao, X. Through plate joints to elliptical and circular hollow sections. In *Tubular Structures XI, Proceedings of the 11th International Symposium and IIW International Conference on Tubular Structures*, Quebec City, QC, Canada; Routledge: London, UK, 2017; pp. 221–228.
23. Zhao, X. Branch Plate Connections to Elliptical Hollow Sections. Master’s Thesis, University of Toronto, Toronto, ON, Canada, 2005.
24. Mirghaderi, S.R.; Torabian, S.; Keshavarzi, F. I-beam to box-column connection by a vertical plate passing through the column. *Eng. Struct.* **2010**, *32*, 2034–2048. [[CrossRef](#)]
25. Voth, A.P.; Packer, J.A. Branch Plate-to-Circular Hollow Structural Section Connections. I: Experimental Investigation and Finite-element Modeling. *ASCE J. Struct. Eng.* **2012**, *138*, 1007–1018. [[CrossRef](#)]
26. Voth, A.P. Branch Plate-to-Circular Hollow Structural Section Connections. Ph.D. Thesis, University of Toronto, Toronto, ON, Canada, 2010.
27. Di Benedetto, S.; Latour, M.; Rizzano, G. Chord failure resistance of 3D cut welded connections with CHS columns and through I-beams. *Thin-Walled Struct.* **2020**, *154*, 106821. [[CrossRef](#)]
28. Di Benedetto, S.; Latour, M.; Rizzano, G. Assessment of the stiffness of 3D cut welded connections with CHS columns and through I-beams. *Structures* **2020**, *27*, 247–258. [[CrossRef](#)]
29. Piscini, A. Passing-Through Tubular Column Joints for Steel and Composite Constructions Made by Laser Cutting Technology. Ph.D. Thesis, Università di Pisa, Pisa, Italy, 2019.
30. Kanyilmaz, A. The problematic nature of steel hollow section joint fabrication, and a remedy using laser cutting technology: A review of research, applications, opportunities. *Eng. Struct.* **2019**, *183*, 1027–1048. [[CrossRef](#)]
31. Kanyilmaz, A.; Castiglioni, C.A. Fabrication of laser cut I-beam-to-CHS-column steel joints with minimized welding. *J. Constr. Steel Res.* **2018**, *146*, 16–32. [[CrossRef](#)]
32. Das, R.; Castiglioni, C.; Couchaux, M.; Hoffmeister, B.; Degee, H. Design and analysis of laser-cut based moment resisting passing-through I-beam-to-CHS column joints. *J. Constr. Steel Res.* **2020**, *169*, 106015. [[CrossRef](#)]
33. Das, R.; Kanyilmaz, A.; Couchaux, M.; Hoffmeister, B.; Degee, H. Characterization of moment resisting I-beam to circular hollow section column connections resorting to passing-through plates. *Eng. Struct.* **2020**, *210*, 110356. [[CrossRef](#)]
34. DIANA. *DIANA User’s Manual, DIANA Release 10.2*; DIANA FEA BV: Delft, The Netherlands, 2018; Available online: <https://dianafea.com/> (accessed on 3 September 2023).
35. Couchaux, M.; Castiglioni, C.; Hjiaj, M.; Wald, F. I-beam-to-CHS-column moment resisting joints using passing-through plates. *J. Constr. Steel Res.* **2021**, *184*, 106703. [[CrossRef](#)]
36. Couchaux, M.; Vyhlas, V.; Kanyilmaz, A.; Hjiaj, M. Passing-through I-beam-to-CHS column joints made by laser cutting technology: Experimental tests and design model. *J. Constr. Steel Res.* **2021**, *176*, 106298. [[CrossRef](#)]
37. Kanyilmaz, A.; Castiglioni, C.A.; Menghini, A. *LASer Cutting Technology for Tubular Structures*; Mid-Term Report, EU-RFCS Research Project; Grant Agreement Number 101034038; DABC: Milan, Italy, 2023.
38. Safaeifaegh, S.; Zanon, G.; Bursi, O.S. Study of the behaviour of S355 welded joints with CHS columns and through beams. *ce/Pap.—Proc. Civ. Eng.* **2023**, *6*, 1513–1518. [[CrossRef](#)]
39. Shamlooeei, M.; Zanon, G.; Brugnolli, M.; Bursi, O.S. Study of the effects of laser cutting processes on S235 structural steel. *ce/Pap.—Proc. Civ. Eng.* **2023**, *6*, 2521–2526. [[CrossRef](#)]

Disclaimer/Publisher’s Note: The statements, opinions and data contained in all publications are solely those of the individual author(s) and contributor(s) and not of MDPI and/or the editor(s). MDPI and/or the editor(s) disclaim responsibility for any injury to people or property resulting from any ideas, methods, instructions or products referred to in the content.